# Supporting Information

## Efficient Through-Space Charge Transfer in Heavy-Atom-Free Triplet Photosensitizers via Conformational Preorganization

Guizhen Ma, Heng Wu, and Hui-Qing Peng*

State Key Laboratory of Chemical Resource Engineering, Beijing Advanced Innovation Center for Soft Matter Science and Engineering, Beijing University of Chemical Technology, North Third Ring Road, Beijing 100029, China;

*Corresponding author: hqpeng@mail.buct.edu.cn (Hui-Qing Peng)

## Experimental Section/Methods

### Materials and Instruments.

All reagents were purchased from commercial suppliers (Energy Chemical, Bidepharm, Sigma-Aldrich, TCI) and used without further purification. $^{1}$H NMR and $^{13}$C NMR spectra were measured on a Bruker Advance III (400 MHz) instrument using $CDCl_3$, or DMSO-$d_6$ as the solvent and tetramethylsilane as the internal reference. HRMS spectra were acquired on a Thermo Scientific Orbitrap Exploris 120 mass spectrometer operating in positive ion mode at a resolution of 60,000 (at m/z 200). UV-vis absorption spectra were measured by a SHIMADZU UV-2600i spectrophotometer. The photoluminescence spectra were measured by a SHIMADZU RF-6000 spectro fluorophotometer. ROS assays were conducted by using a Xenon lamp (Microsolar300, Beijing Perfectlight). ESR analysis was performed on a Bruker E 500 spectrometer. The Photopolymerization reaction was carried out under LED light irradiation (420-650 nm) with a light power density of 43 mW·cm$^{-2}$.

### Methods.

### Lippert−Mataga (LM) equation Calculations.

$$\Delta\nu = \nu_{abs} - \nu_{em} = \frac{1}{4\pi\varepsilon_0 hca^3}\frac{2}{(\mu_e - \mu_g)^2}\Delta f + const$$

$$\Delta f = \frac{\varepsilon - 1}{2\varepsilon + 1} - \frac{n^2 - 1}{2n^2 + 1}$$

where $\Delta\nu$ is the Stokes shift, the difference in energy between the absorption and emission maxima; $\nu_{abs}$ and $\nu_{em}$ are the wavenumbers of absorption and emission peaks, respectively; $h$ is Planck's constant; $c$ is the speed of light; $a$ is the Onsager cavity radius in which the chromophore resides; and $\Delta\mu = \mu_e - \mu_g$ is the difference between the excited-state and ground-state dipole moments as presented by the Equation 1; $\Delta f$ is the orientational polarizability of solvent which could be deduced from the dielectric constant ε and the refractive index $n$ of the solvent represented by the Equation 2. Accordingly, if $\Delta\mu$ was independent of the solvent polarity, a straight line would be obtained for $\Delta\nu$ versus $\Delta f$.

### Determination of $^{1}O_2$ Quantum Yield.

9,10-anthracenediyl-bis(methylene) dimalonic acid (ABDA)was used for the detection of $^1O_2$. Compounds (10 μM) were dissolved in 2 mL water containing 100 μM of ABDA. The mixture was irradiated under white light (35 mW·cm$^{-2}$) irradiation. The absorbance decrease of ABDA at 378 nm was recorded at various irradiation time.

**Detection of ROS production.**

2,7-dichlorodihydrofluorescein (DCFH) was used as an indicator for the detection of ROS in the solution. When ROS is generated in the system, the non-fluorescent DCFH will be oxidized and emit obvious fluorescence at 524 nm. Compounds (10 μM) were dissolved in 2 mL water containing 10 μM of DCFH. The mixture was then placed in a cuvette and irradiated under white light (35 mW·cm$^{-2}$) irradiation. The fluorescence intensity change of the sample at 524 nm was recorded by the fluorescence spectrometer.

**Detection of $O_2^{\bullet-}$ production.**

Dihydrorhodamine 123 (DHR123) was used as an indicator for the detection of $O_2^{\bullet-}$ in solution. When $O_2^{\bullet-}$ is generated in the system, the DHR 123 will be oxidized and emit strong fluorescence centered at 526 nm. Compounds (10 μM) were dissolved in 2 mL water containing 30 μM of DHR 123. The mixture was irradiated under white light (35 mW·cm$^{-2}$) irradiation. The fluorescence change of the sample at 526 nm was recorded by the fluorescence spectrometer.

**Electron paramagnetic resonance (EPR) Measurement.**

EPR measurement was used to identify the type of ROS using 2,2,6,6-tetramethylpiperidine (TEMP) as the $^1O_2$ indicator, 5,5-dimethyl-1-pyrroline-N-oxide (DMPO) as the $O_2^{\bullet-}$ indicator. For $^1O_2$ and $O_2^{\bullet-}$detection, samples were prepared by mixing 200 μL, 500 μM of compounds and 10 μL TEMP or 0.2 M DMPO in DMF, respectively. And α-phenyl-N-tert-butylnitrone (PBN) as the phenyl radical indicator. For phenyl-radical detection, samples were prepared by dissolving the photocatalyst (0.01 mol%), PBN (5 mM), and DPI (0.5 mol%) in acetonitrile, followed by Ar purging to remove dissolved oxygen. The mixture was then irradiated under white light (35 mW·cm$^{-2}$) for 2 min, and the resulting PBN-Ph spin-adduct signals were recorded by EPR.

**Photocurrent response experiment**

The photocurrent response experiment was conducted using a three-electrode system. The working electrode consisted of an FTO glass electrode coated with a photosensitizer, while the counter electrode and reference electrode were platinum and Ag/AgCl electrodes, respectively. Measurements were performed in 0.01 M phosphate buffer solution under illumination from a white light xenon lamp (200 $mW \cdot cm^{-2}$) at 10-second intervals.

**Charge transfer resistances test**

The charge transfer resistance experiment was conducted using a three-electrode system. A carbon paper electrode coated with photosensitizer was selected as the working electrode, while platinum electrodes and Ag/AgCl electrodes were chosen as the working and reference electrodes, respectively. Measurements were performed in 0.01 M phosphate buffer solution.

**Calculation method**

All the calculations were carried out with Gaussian 09 package unless otherwise specified.[S1] The structures of global minimum points were obtained using density functional theory (DFT, for $S_0$ state) and time-dependent DFT (TD-DFT, for $S_1$ and $T_1$ state) methods with B3LYP/6-31G(d,p) and B3LYP-D3(BJ)/PBE1PBE basis set, respectively.[S2-S5] Hole-electron analysis[S6] and the interaction region indicator (IRI) analysis[S7] were conducted with Multiwfn software.[S8-S9] The root-mean-square deviation (RMSD) of atomic positions of the optimized structures at $S_0$, $S_1$ and $T_1$ states and the visualization of orbitals and iso-surface were realized by VMD software.[S10] The electron and hole analysis and inter fragment charge transfer analysis were performed with Multiwfn 3.7.

**Photopolymerization**

Different concentrations of photocatalyst, diphenyliodonium salt (0.5 mol%) dissolved in a trace amount of organic solvent, were individually mixed with 2 mmol of olefin monomer. Mesitylene (20 μL) was then added to each mixture. The resulting solutions were exposed to light for the desired durations and subsequently dissolved in

deuterated chloroform for $^1$H NMR spectroscopy. Subsequently, the solutions were dissolved in deuterated chloroform for $^1$H NMR spectroscopy. The monomer conversion ratio was determined by using mesitylene as an internal standard and calculating the ratio of the integrated area of the characteristic peaks in the NMR hydrogen spectra. The calculation was performed as follows:

$$\text{Converision (\%)} = 100\% \times \left(1 - \frac{H_t}{H_0}\right)$$

In the above equation, $H_t$ and $H_0$ represent the integrated area of the hydrogen atom featured in the olefin monomers after and before exposure to light for t seconds, respectively.

**Synthesis and Characterization**

**Synthesis of 4,4'-(piperazine-1,4-diyl)dibenzaldehyde (compound 1).**

Piperazine (1.7 g, 20 mmol) and Potassium carbonate (5.52 g, 40 mmol) was added into 200 mL dimethyl sulfoxide in a flask, which was stirred for 10 min to mix evenly. Then 4-fluoro-benzaldehyde (4.96 g, 40 mmol) was dropped in, and the reactant was refluxed for 24 h to finish the reaction. After cooling to room temperature, 300 mL water was added to the mixture to produce a precipitate, then the mixture was filtered to obtain a yellow solid. The yellow solid was recrystallized with dichloromethane and petroleum ether to obtain the product (yellow powder, yield 85%). Compound 1 $^1$H NMR (400 MHz, DMSO-$d_6$) δ 9.74 (s, 2H), 7.75 (d, $J$ = 8.9 Hz, 4H), 7.07 (d, $J$ = 8.9 Hz, 4H), 3.61 (s, 8H).

**Synthesis of PA-DC.**

A dry ethanol solution of compound 1 (58.8 mg, 0.2 mmol) and malononitrile (33.03 mg, 0.5 mmol) with a few drops of piperidine was refluxed overnight under nitrogen. After cooling the solution to room temperature, a deep red precipitate was formed. It was collected by filtration, washed with DCM for three times, then dried under vacuum at 40 ℃ to a constant weight. Finally, PA-DC was obtained in a yield of 89%. PA-DC $^1$H NMR (400 MHz, DMSO-$d_6$) δ 8.13 (s, 2H), 7.89 (d, $J$ = 9.0 Hz, 4H), 7.07 (s, 4H), 3.75 (s, 8H). $^{13}$C NMR (101 MHz, DMSO-$d_6$) δ 159.5, 154.2, 134.1, 120.4, 116.4, 115.7, 113.2, 70.9, 45.3. MS: m/z $[M+H]^+$ calculated for $C_{24}H_{18}N_6$, 391.1666;

found, 391.1666.

**Synthesis of 4,4'-(ethane-1,2-diylbis(methylazanediyl))dibenzaldehyde (compound 2).**

N,N'-Dimethyl-1,2-ethanediamine (1.76 g, 20 mmol) and Potassium carbonate (5.52 g, 40 mmol) was added into 200 mL dimethyl sulfoxide in a flask, which was stirred for 10 min to mix evenly. Then 4-fluoro-benzaldehyde (4.96 g, 40 mmol) was dropped in, and the reactant was refluxed for 24 h to finish the reaction. After cooling to room temperature, 300 mL water was added to the mixture to produce a precipitate, then the mixture was filtered to obtain a yellow solid. The yellow solid was recrystallized with dichloromethane and petroleum ether to obtain the product (yellow powder, yield 85%). Compound 2 $^{1}$H NMR (400 MHz, DMSO-$d_6$) δ 9.67 (s, 2H), 7.66 (d, $J$ = 8.3 Hz, 4H), 6.77 (d, $J$ = 8.5 Hz, 4H), 3.71 (s, 4H), 2.98 (s, 6H).

**Synthesis of DM-DC.**

A dry ethanol solution of compound 2 (58.8 mg, 0.2 mmol) and malononitrile (33.03 mg, 0.5 mmol) with a few drops of piperidine was refluxed overnight under nitrogen. After cooling the solution to room temperature, a deep red precipitate was formed. It was collected by filtration, washed with DCM for three times, then dried under vacuum at 40 ℃ to a constant weight. Finally, DM-DC was obtained in a yield of 89%. DM-DC $^{1}$H NMR (400 MHz, DMSO-$d_6$) δ 8.06 (s, 2H), 7.80 (s, 4H), 6.82 (s, 4H), 3.79 (s, 4H), 3.04 (s, 6H). $^{13}$C NMR (101 MHz, DMSO-$d_6$ + $CH_3COOH$) δ 159.1, 153.8, 139.2, 134.0, 119.6, 112.1, 83.2, 49.2, 24.7, 17.8. MS: m/z $[M+H]^+$ calculated for $C_{24}H_{20}N_6$, 393.1823, 394.1856; found, 393.1876, 394.1897.

**Synthesis of EM-DC.**

A dry ethanol solution of 4-Dimethylaminobenzaldehyde (30.0 mg, 0.2 mmol) and Malononitrile (16.5 mg, 0.25 mmol) with a few drops of piperidine was refluxed overnight under nitrogen. After cooling the solution to room temperature, a deep red precipitate was formed. It was collected by filtration, washed with DCM for three times, then dried under vacuum at 40 ℃ to a constant weight. EM-DC was obtained in yield of 85%. EM-DC $^{1}$H NMR (400 MHz, DMSO-$d_6$) δ 8.05 (s, 1H), 7.84 (d, $J$ = 9.1 Hz, 2H), 6.86 (d, $J$ = 9.2 Hz, 2H), 3.11 (s, 6H). $^{13}$C NMR (101 MHz, Chloroform-$d$) δ 158.1,

154.2, 133.8, 119.3, 116.0, 114.9, 111.6, 72.0, 40.1. MS: m/z $[M+H]^+$ calculated for $C_{12}H_{11}N_3$, 198.1026; found, 198.1018.

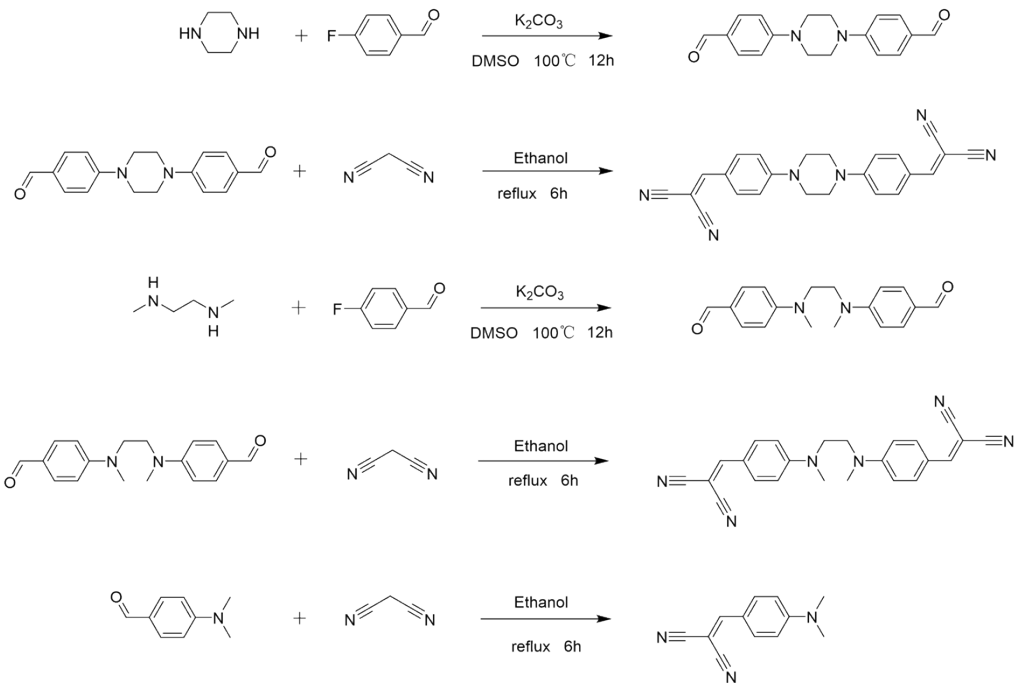


**Scheme S1.** Synthetic route of Compound 1, PA-DC, Compound 2, DM-DC and EM-DC.

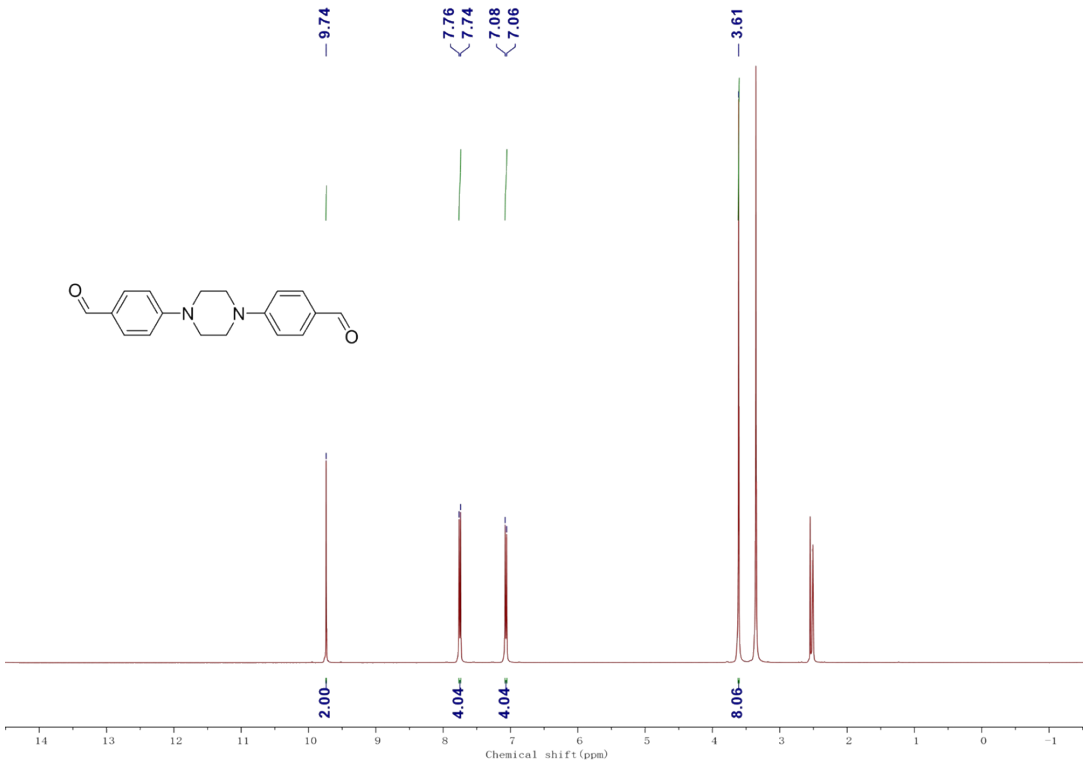


**Fig. S1** $^1$H NMR spectrum of Compound 1 in DMSO-$d_6$.

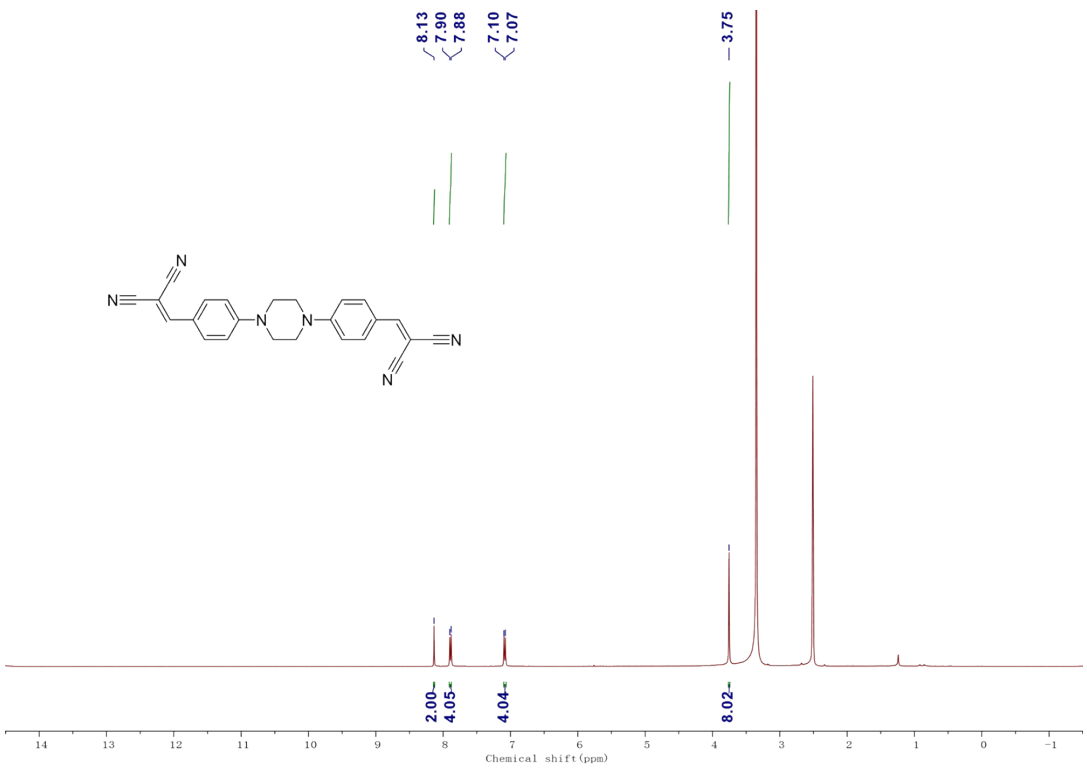


**Fig. S2** $^{1}$H NMR spectrum of PA-DC in DMSO-$d_6$.

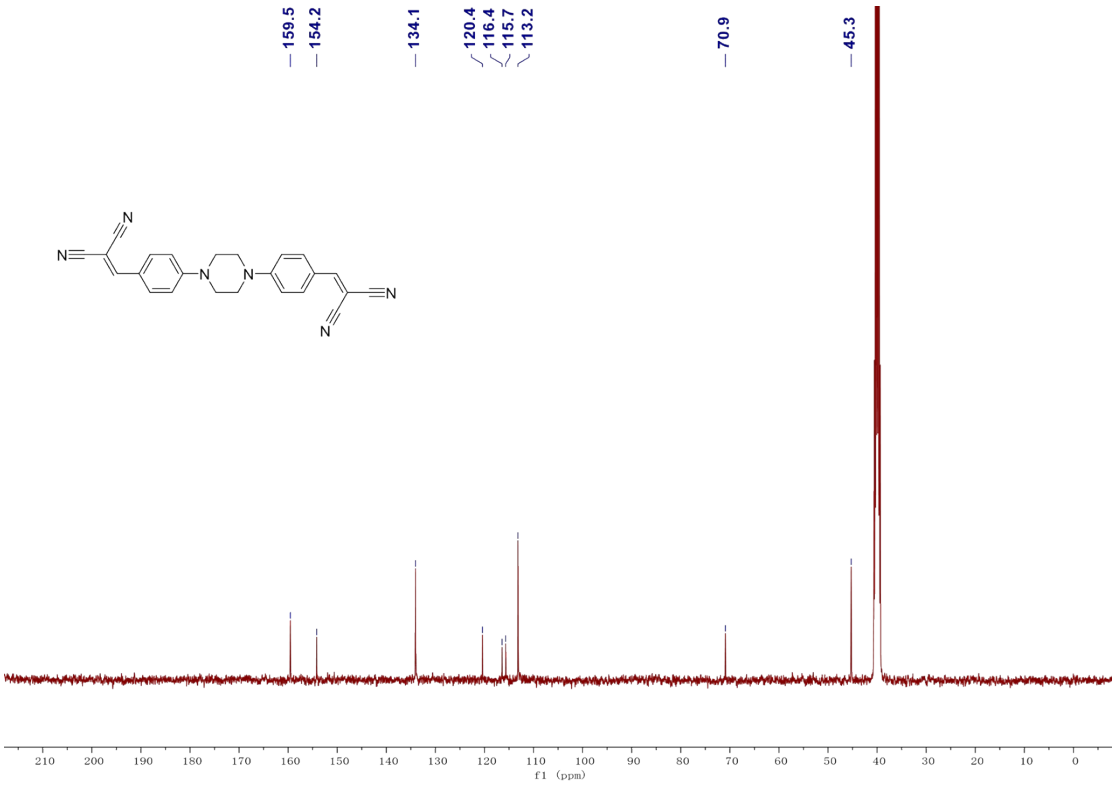


**Fig. S3** $^{13}$C NMR spectrum of PA-DC in DMSO-$d_6$.

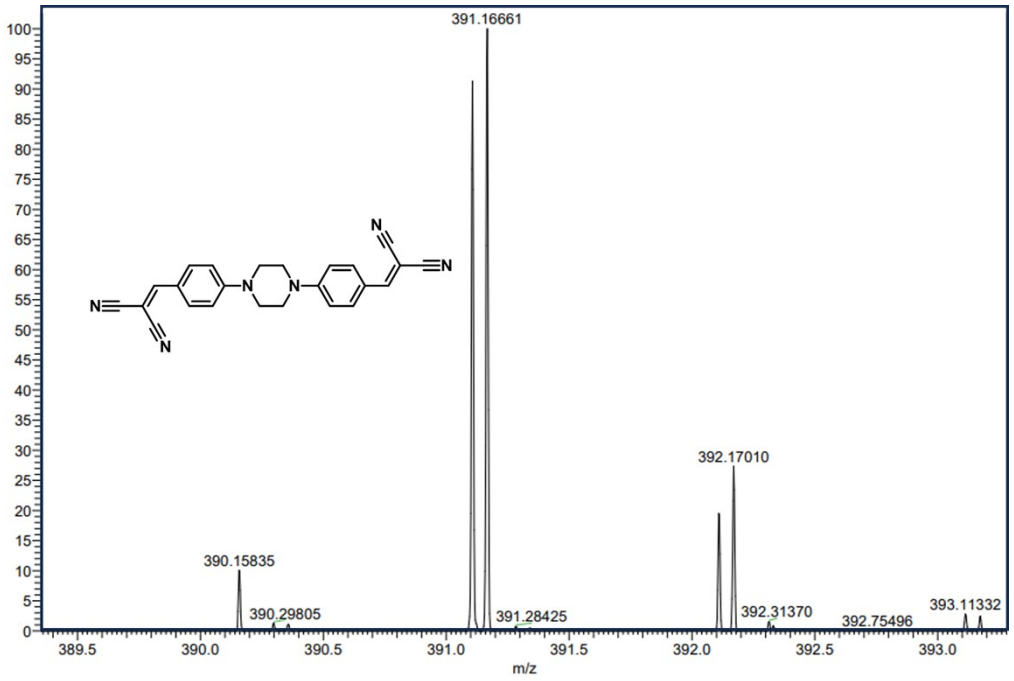


**Fig. S4** HRMS spectrum of PA-DC in acetonitrile.

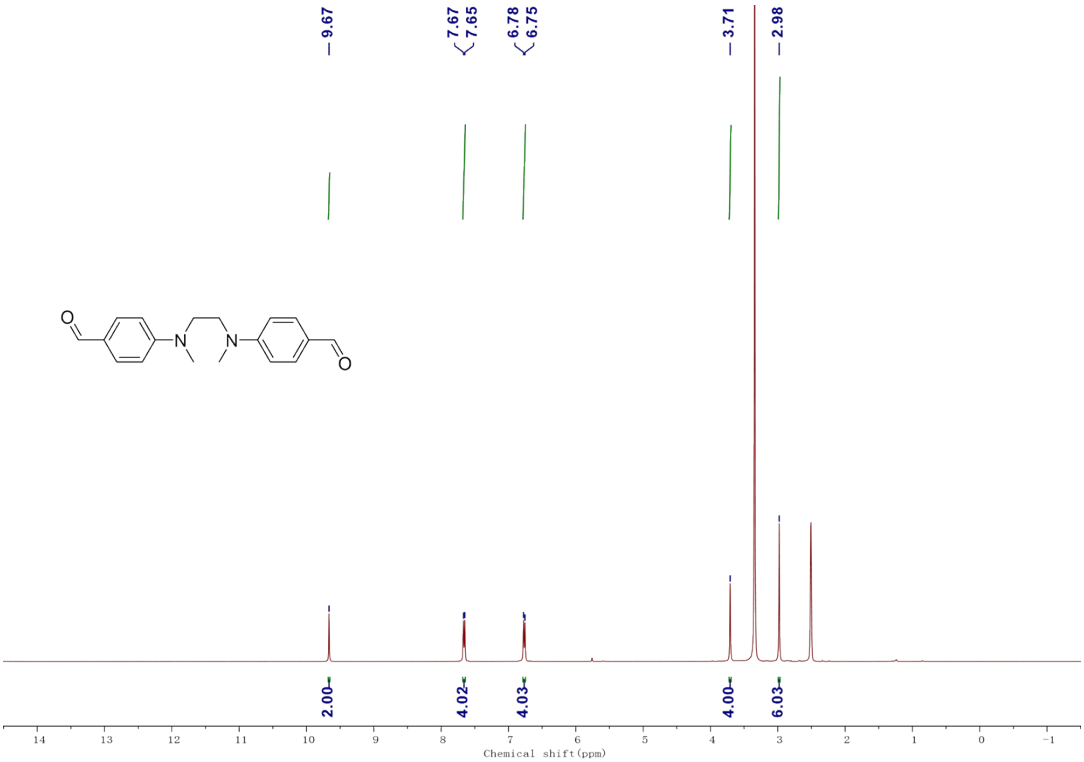


**Fig. S5** $^{1}$H NMR spectrum of Compound 2 in DMSO-$d_6$.

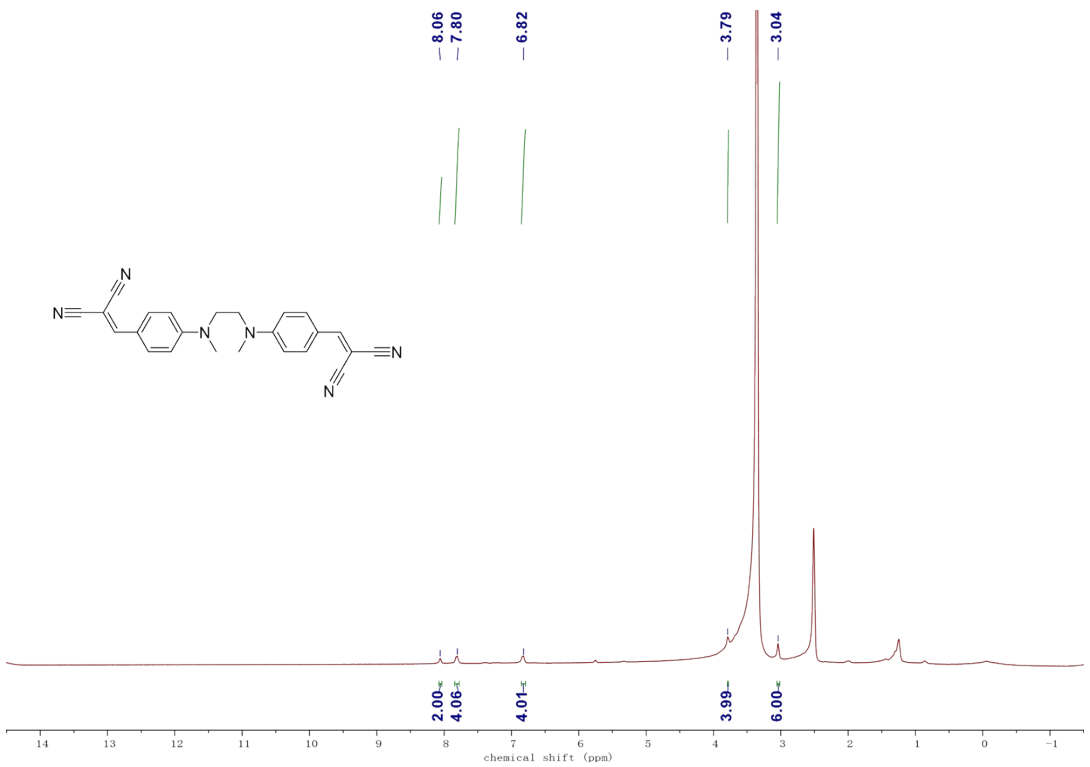


**Fig. S6** $^{1}$H NMR spectrum of DM-DC in DMSO-$d_6$.

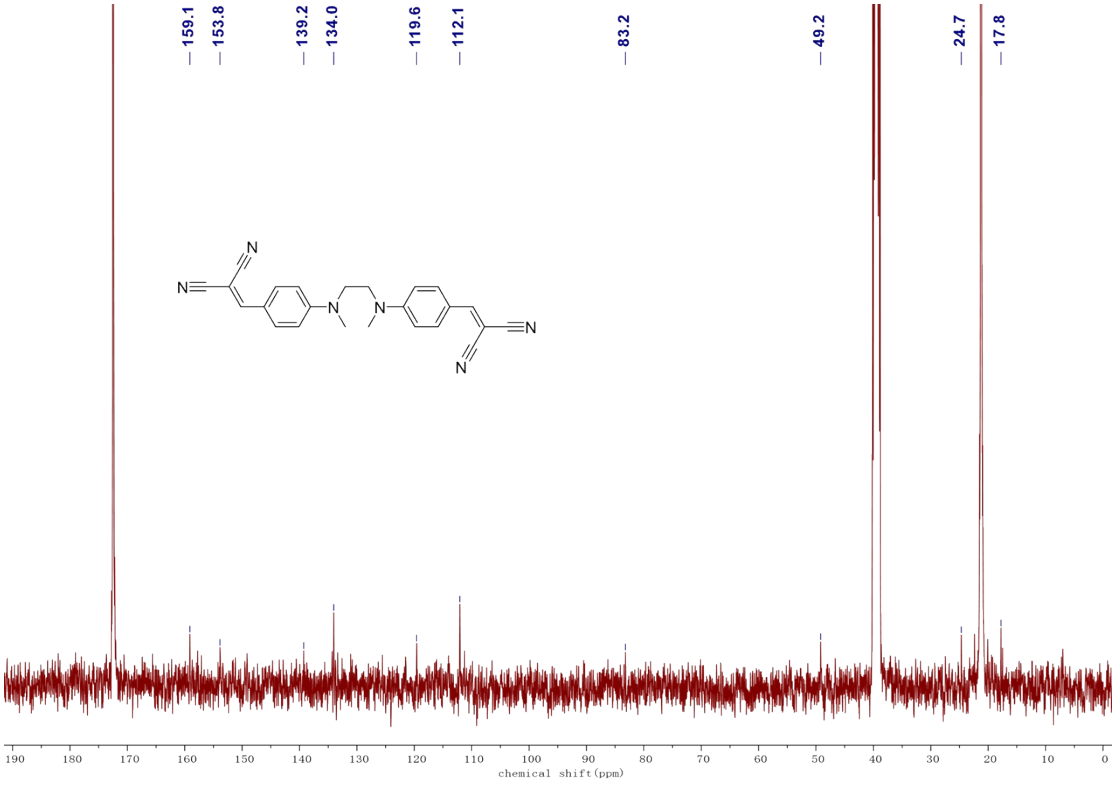


**Fig. S7** $^{13}$C NMR spectrum of DM-DC in DMSO-$d_6$ with $CH_3COOH$ added as a cosolvent.

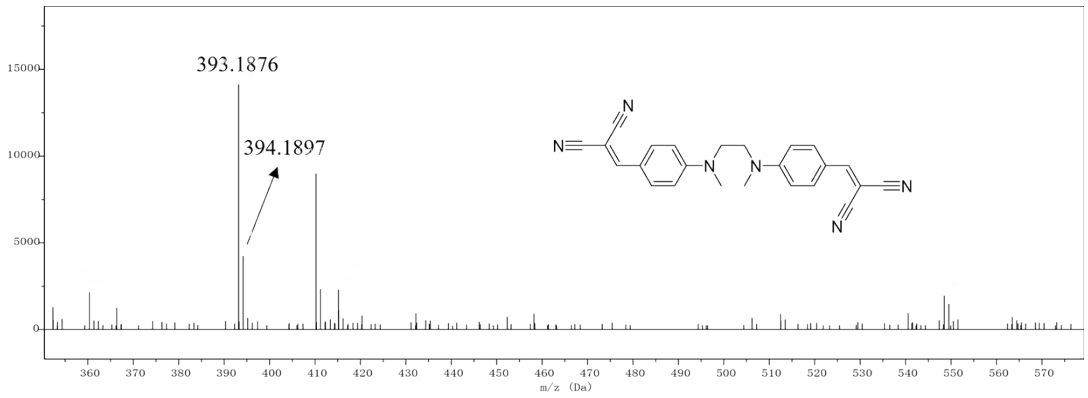


**Fig. S8** HRMS spectrum of DM-DC in acetonitrile.

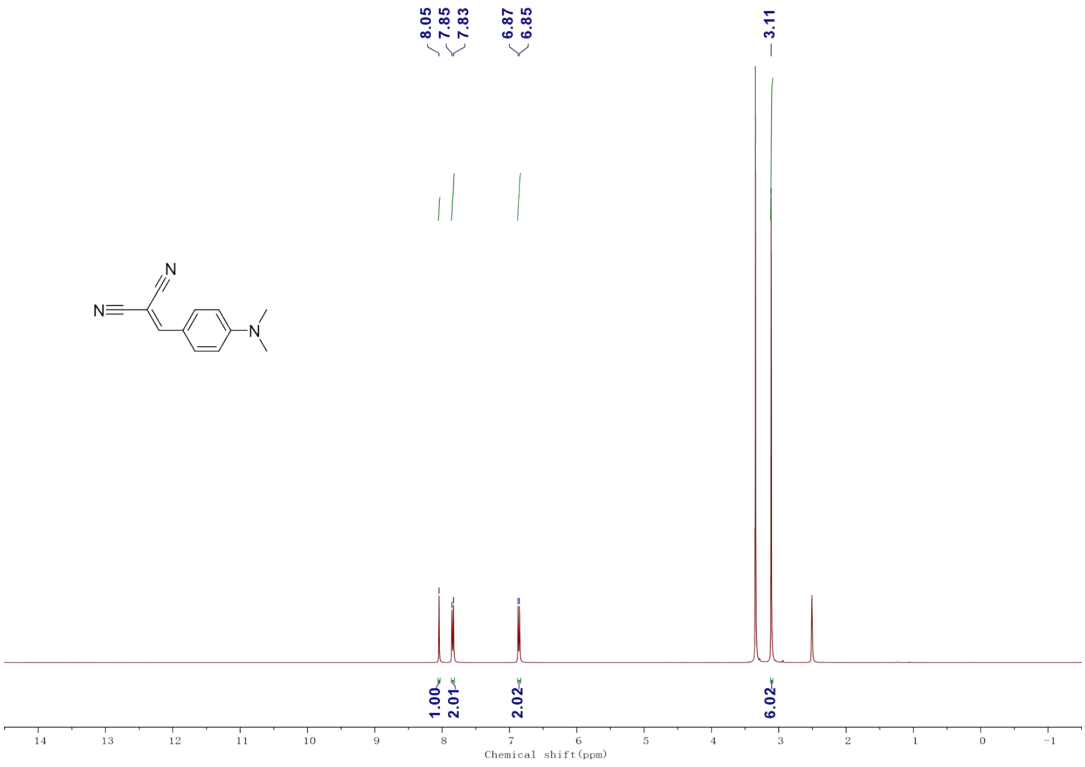


**Fig. S9** $^{1}$H NMR spectrum of EM-DC in DMSO-$d_6$.

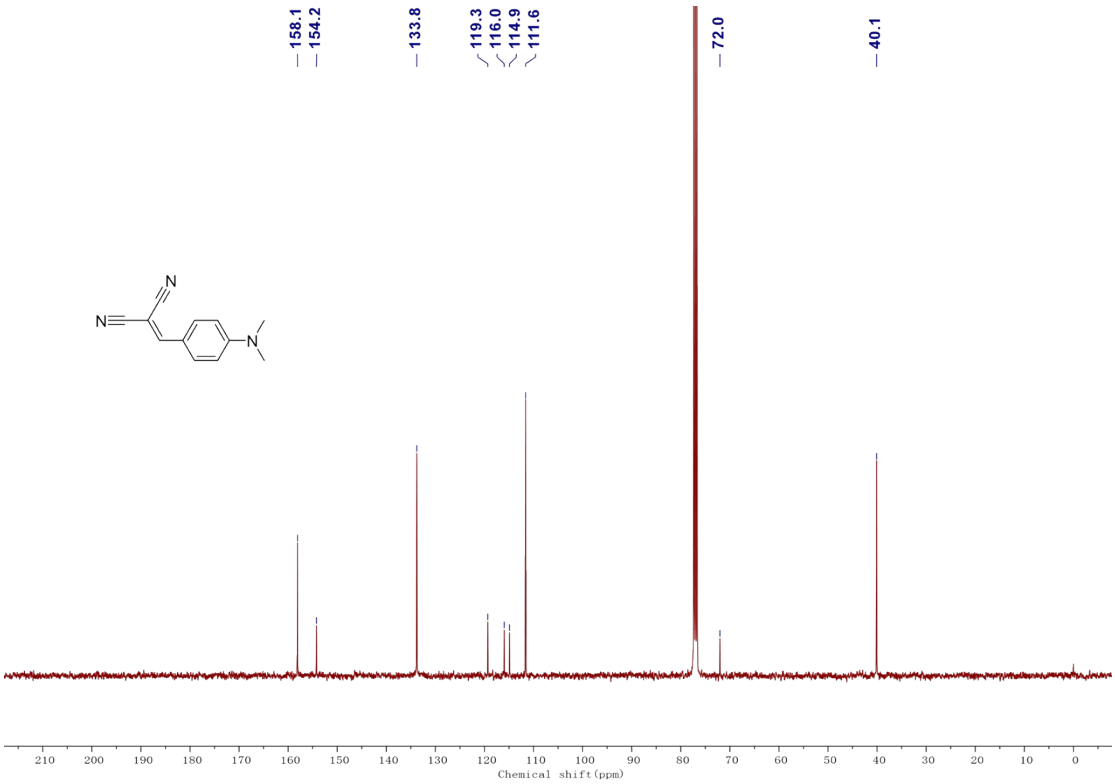


**Fig. S10** $^{13}$C NMR spectrum of EM-DC in Chloroform-*d*.

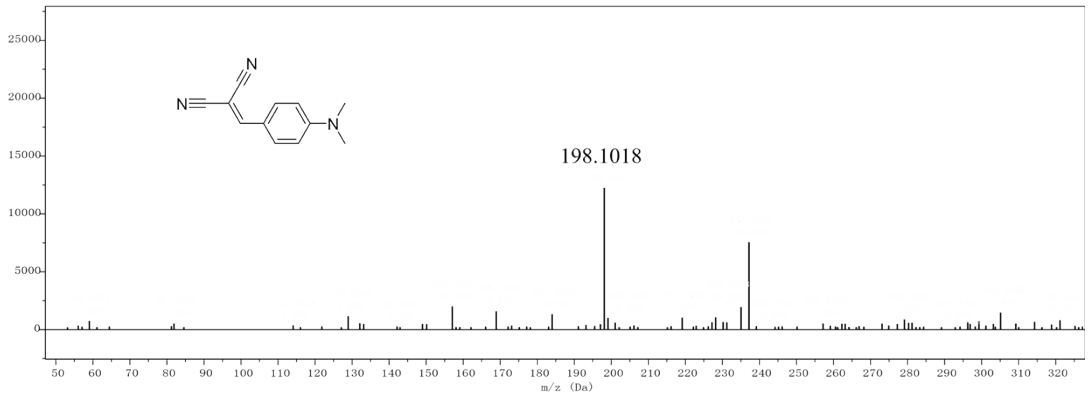


**Fig. S11** HRMS spectrum of EM-DC in acetonitrile.

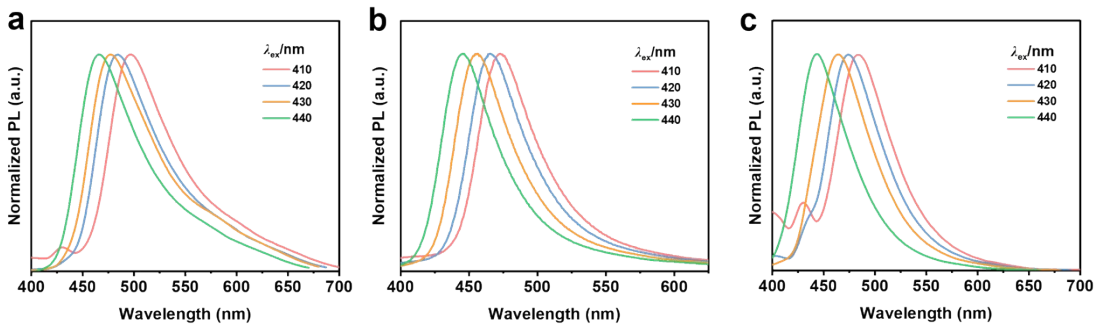


**Fig. S12** Normalized PL spectra of DM-DC (a), PA-DC (b), and EM-DC (c) at different excitation wavelengths ($\lambda_{ex}$) in acetone (c = $1\times10^{-5}$ M).

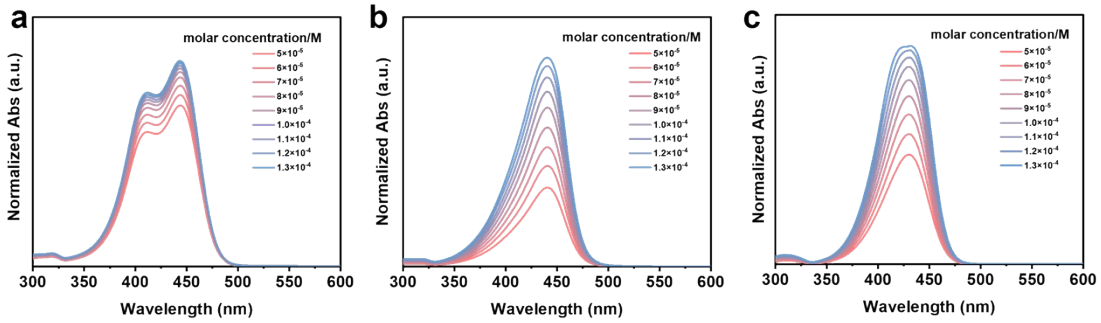


**Fig. S13** Normalized concentration-dependent absorption spectra of DM-DC (a), PA-DC (b), and EM-DC (c) in acetonitrile, with concentrations increasing from $5.0\times10^{-5}$ M to $1.4\times10^{-4}$ M.

| | $k_1$ | $k_2$ | $k_2/k_1$ |
|---|---|---|---|
| **DM-DC** | 0.0840 | 1.2035 | 14.3 |
| **PA-DC** | -0.0116 | 0.0392 | 3.38 |

**Table S1.** $k_1$ is the slope of $I/I_0$ with $f_w$ from 0% to 50%; $k_2$ is the slope of $I/I_0$ with $f_w$ from 50% to 80%.

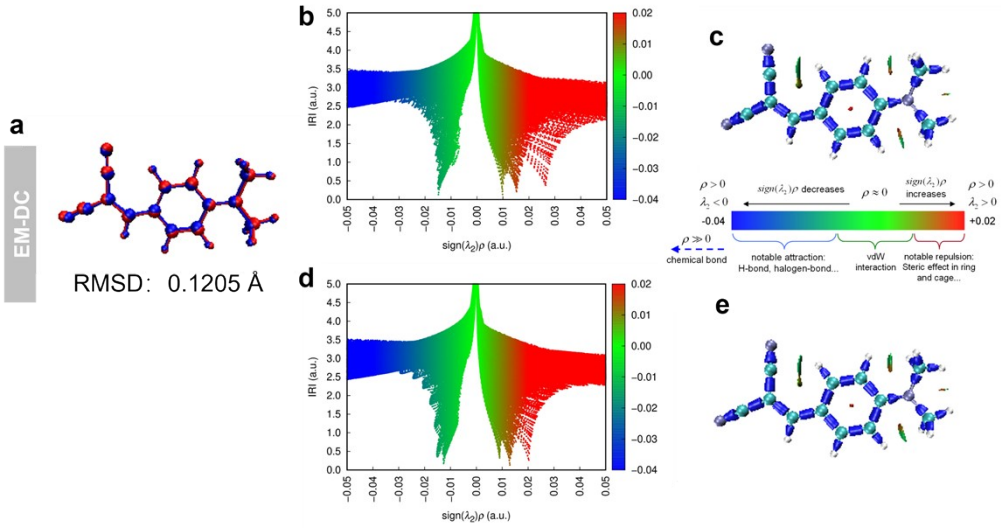


**Fig. S14** Overlaps of the optimized ground-state (blue) and excited-state (red) geometries of EM-DC. The root-mean-square deviation (RMSD) of atomic positions was calculated to evaluate the extent of intramolecular motions (a). Interaction regions and the corresponding scatter plots depict the intramolecular interactions of EM-DC in its optimized ground-state (b, c) and excited-state (d, e) geometries, as analyzed by the interaction region indicator (IRI). The IRI isosurfaces are colored according to the sign($\lambda_2$)ρ function, with red, green, and blue denoting repulsion, significant interaction,

and attraction, respectively (vdW denotes van der Waals interactions).

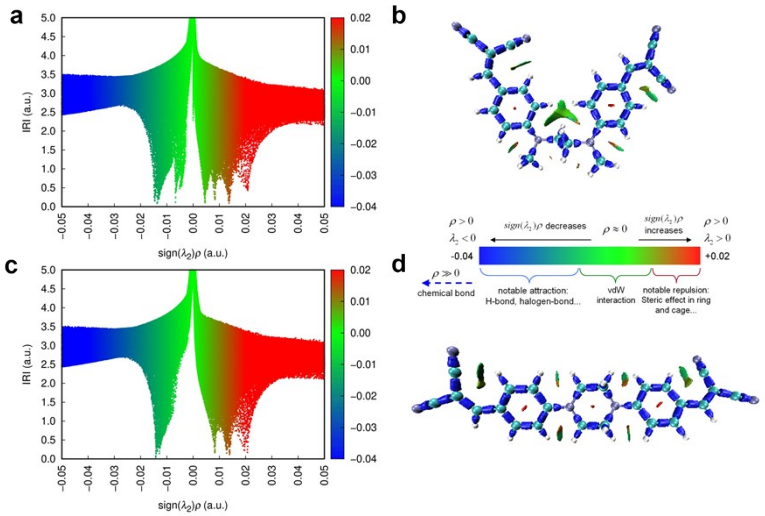


**Fig. S15** Interaction regions and corresponding scatter plots depict intramolecular interactions within DM-DC (a, b) and PA-DC (c, d) in their optimized ground-state geometries, as analyzed by the interaction region indicator (IRI). The IRI isosurfaces are colored according to the sign($\lambda_2$)ρ function, with red, green, and blue representing repulsion, significant interaction, and attraction, respectively (vdW denotes van der Waals interactions).

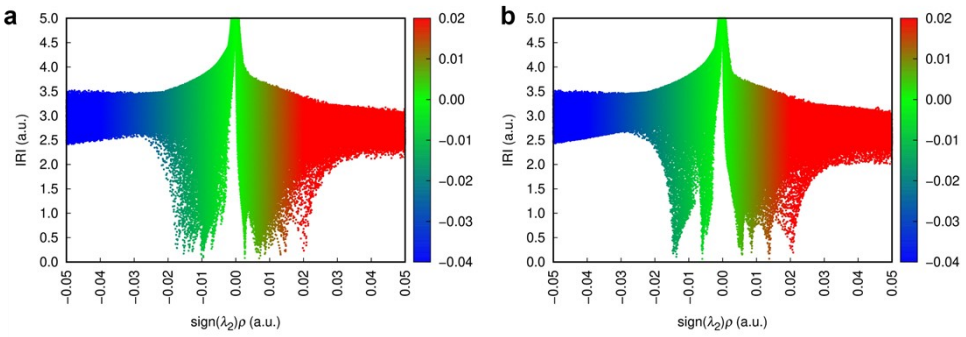


**Fig. S16** Corresponding scatter plots depict intramolecular interactions within DM-DC (a) and PA-DC (b) in their optimized excited-state geometries, as analyzed by the interaction region indicator (IRI). The IRI isosurfaces are colored according to the sign($\lambda_2$)ρ function, with red, green, and blue representing repulsion, significant interaction, and attraction, respectively (vdW denotes van der Waals interactions).

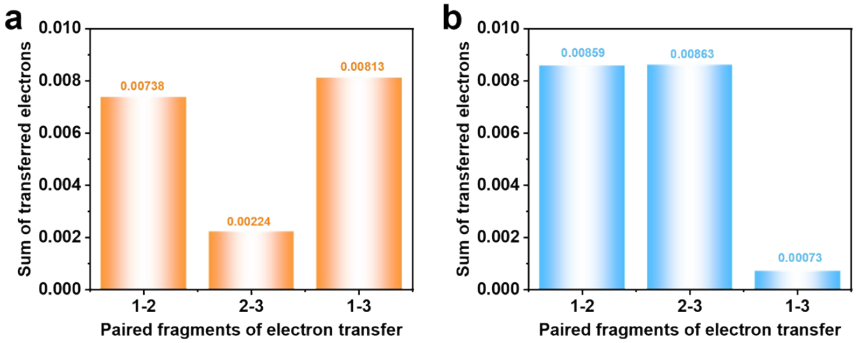


**Fig. S17** Inter-fragment charge-transfer (IFCT) analysis quantifies the contributions of holes and electrons from individual molecular fragments to the $S_0$-$S_1$ transition for DM-DC (a) and PA-DC (b), calculated at their optimized ground-state geometries.

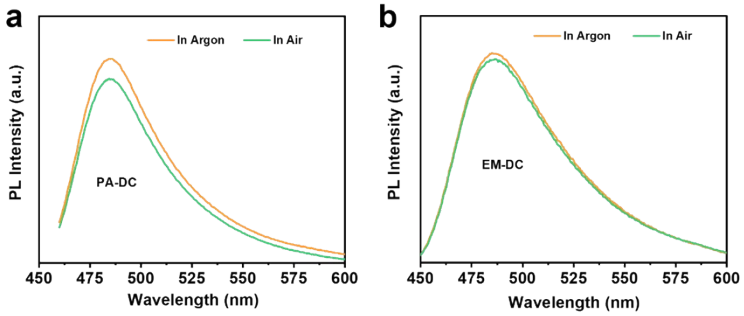


**Fig. S18** PL spectra of PA-DC (a) and EM-DC (b) in acetonitrile before and after deoxygenation. Conditions: concentration = $1\times10^{-5}$ M.

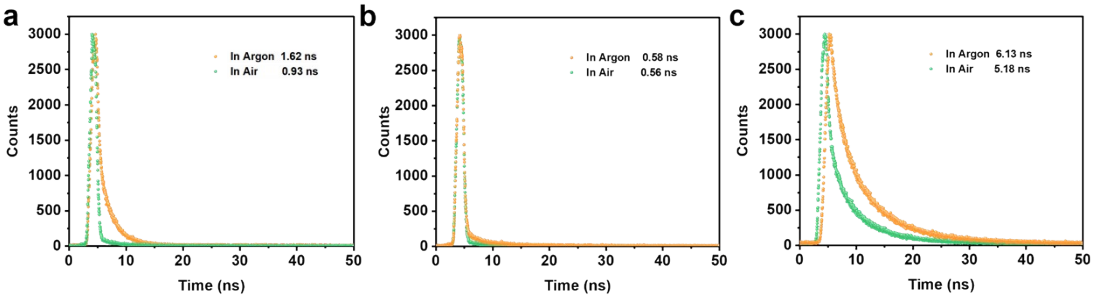


**Fig. S19** Fluorescence decay curves of DM-DC (a), PA-DC (b), and EM-DC (c) monitored at their respective emission maxima in acetonitrile before and after deoxygenation.

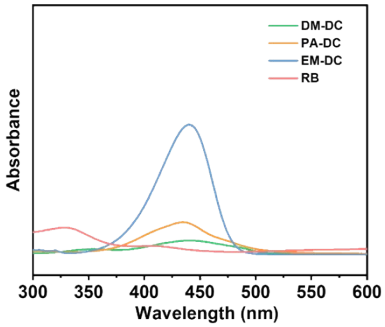


**Fig. S20** Absorption spectra of DM-DC, PA-DC, EM-DC, and RB in water. ($c = 1\times10^{-5}$ M).

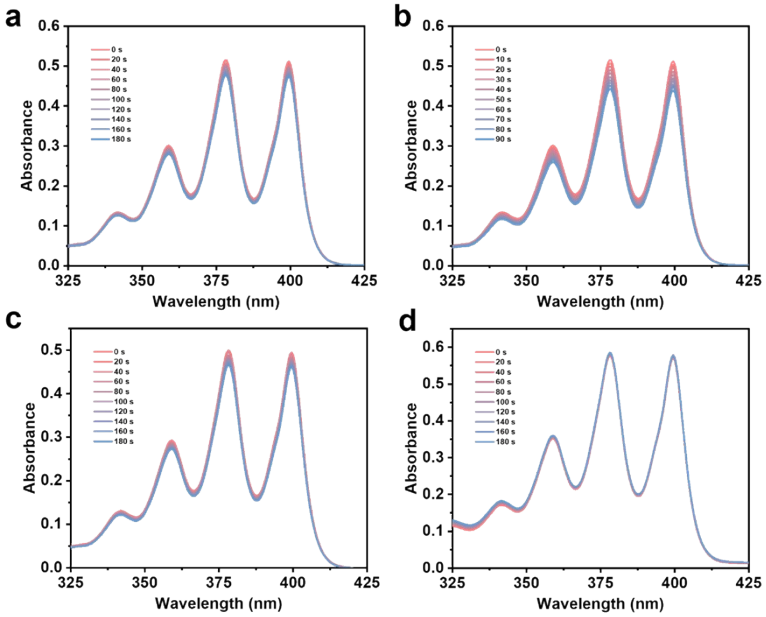


**Fig. S21** Absorption spectra of ABDA solutions in the presence of DM-DC (a), PA-DC (b), EM-DC (c), and RB (d) under dark conditions for different times (ABDA: 100 μM; DM-DC, PA-DC, EM-DC, or RB: 10 μM).

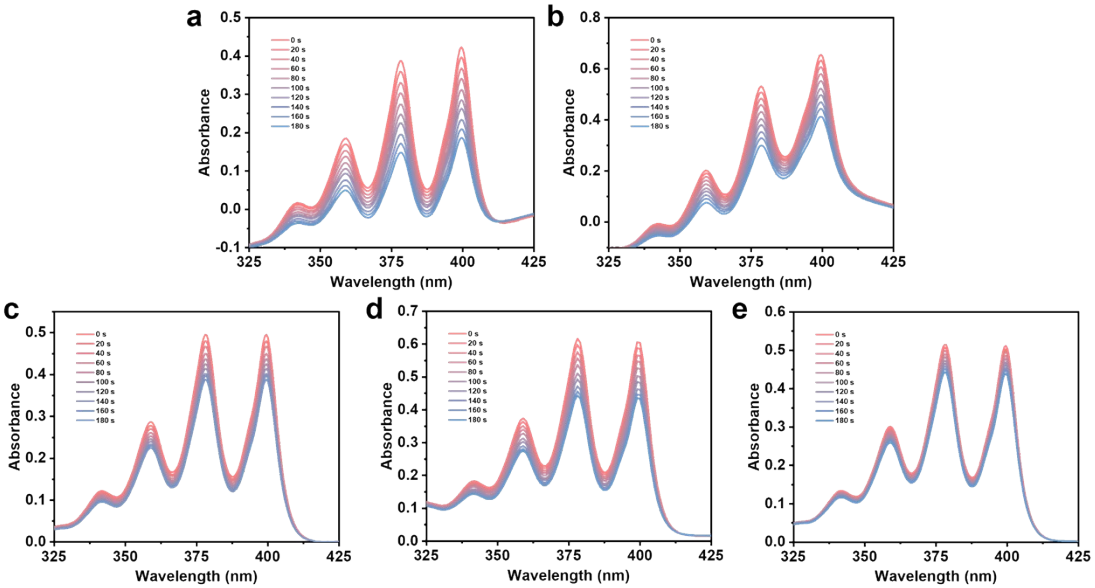


**Fig. S22** Absorption spectra of ABDA solutions in the presence of DM-DC (a), PA-DC (b), EM-DC (c), RB (d), and blank (e) under white light (35 mW·cm$^{-2}$) irradiation for different times (ABDA: 100 μM; DM-DC, PA-DC, EM-DC, or RB: 10 μM).

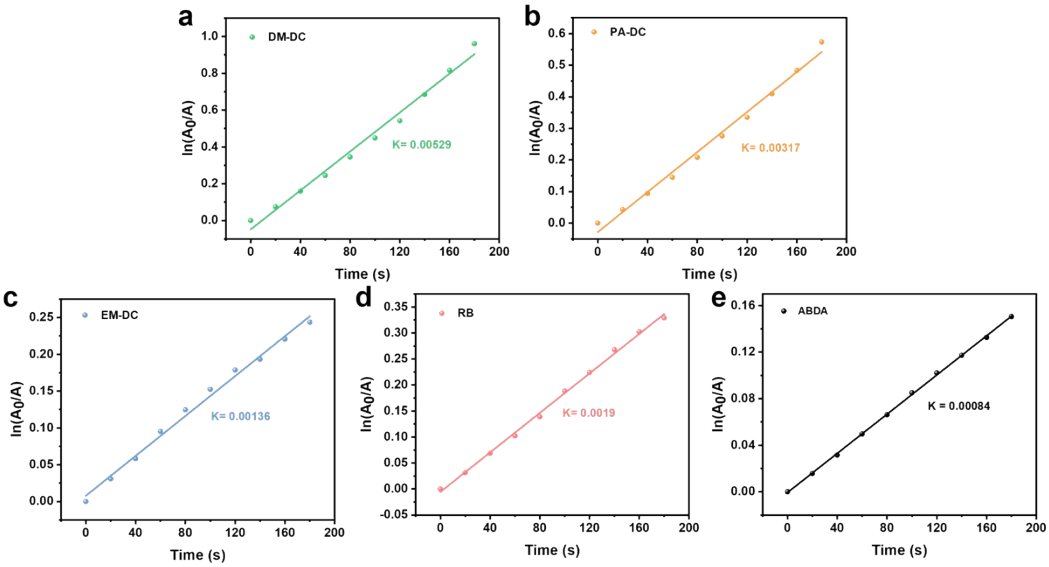


**Fig. S23** First-order kinetics of ABDA absorbance decay, showing the singlet oxygen ($^1O_2$) generation rates of DM-DC (a), PA-DC (b), EM-DC (c), RB (d), and blank (e) under white light (35 mW·cm$^{-2}$) irradiation for different times (ABDA: 100 μM; DM-DC, PA-DC, EM-DC, or RB: 10 μM).

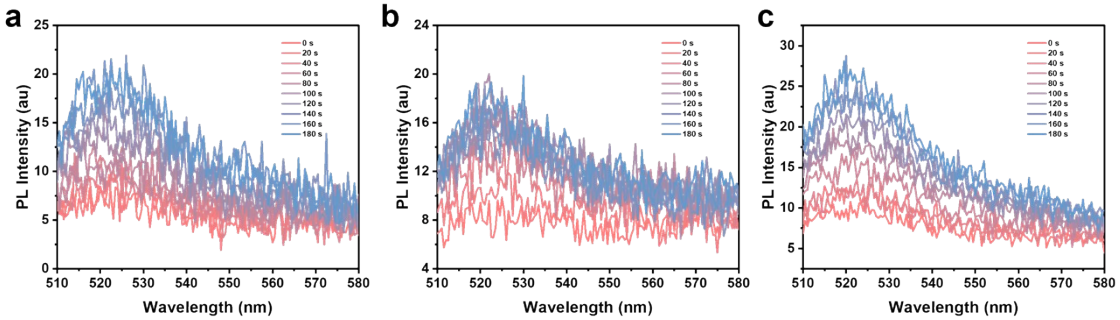


**Fig. S24** PL spectra of DCFH solutions in the presence of DM-DC (a), PA-DC (b), and EM-DC (c) under dark conditions for different times (DCFH: 10 μM; DM-DC, PA-DC, or EM-DC: 10 μM).

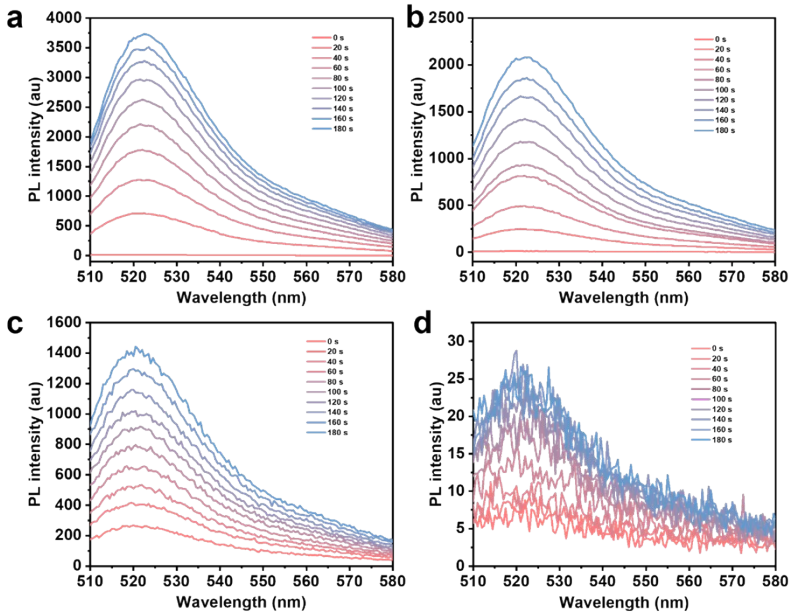


**Fig. S25** PL spectra of DCFH solutions in the presence of DM-DC (a), PA-DC (b), EM-DC (c), and blank (d) under white light (35 mW·cm$^{-2}$) irradiation for different times (DCFH: 10 μM; DM-DC, PA-DC, or EM-DC: 10 μM).

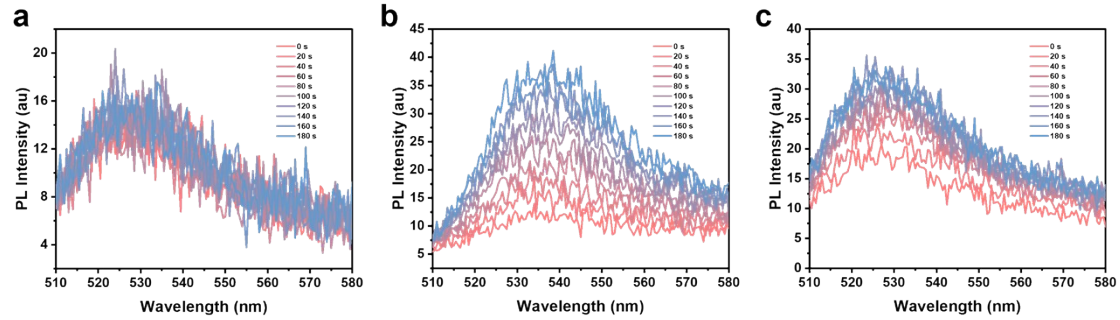


**Fig. S26** PL spectra of DHR123 solutions in the presence of DM-DC (a), PA-DC (b), and EM-DC (c) under dark conditions for different times (DHR123: 30 μM; DM-DC,

PA-DC, or EM-DC: 10 μM).

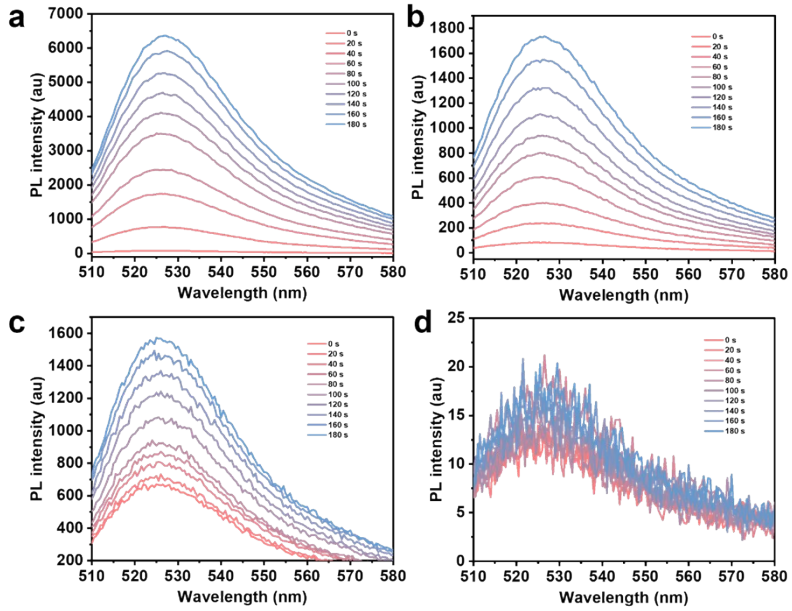


**Fig. S27** PL spectra of DHR123 solutions in the presence of DM-DC (a), PA-DC (b), EM-DC (c), and blank (d) under white light (35 mW·cm$^{-2}$) irradiation for different times (DHR123: 30 μM; DM-DC, PA-DC, or EM-DC: 10 μM).

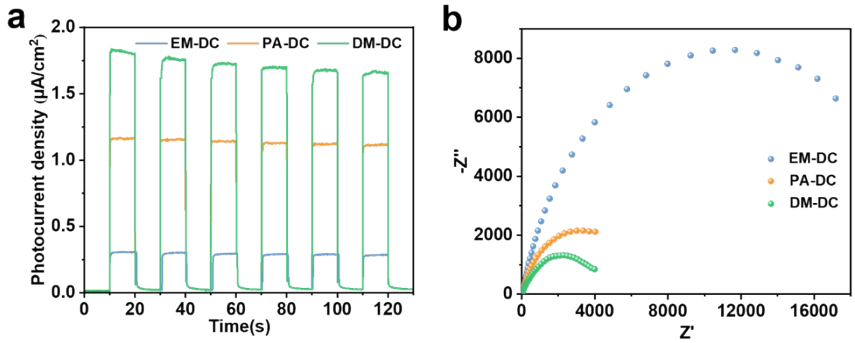


**Fig. S28** (a) Transient photocurrent responses of DM-DC, PA-DC, and EM-DC. (b) Charge transfer resistance of DM-DC, PA-DC, and EM-DC.

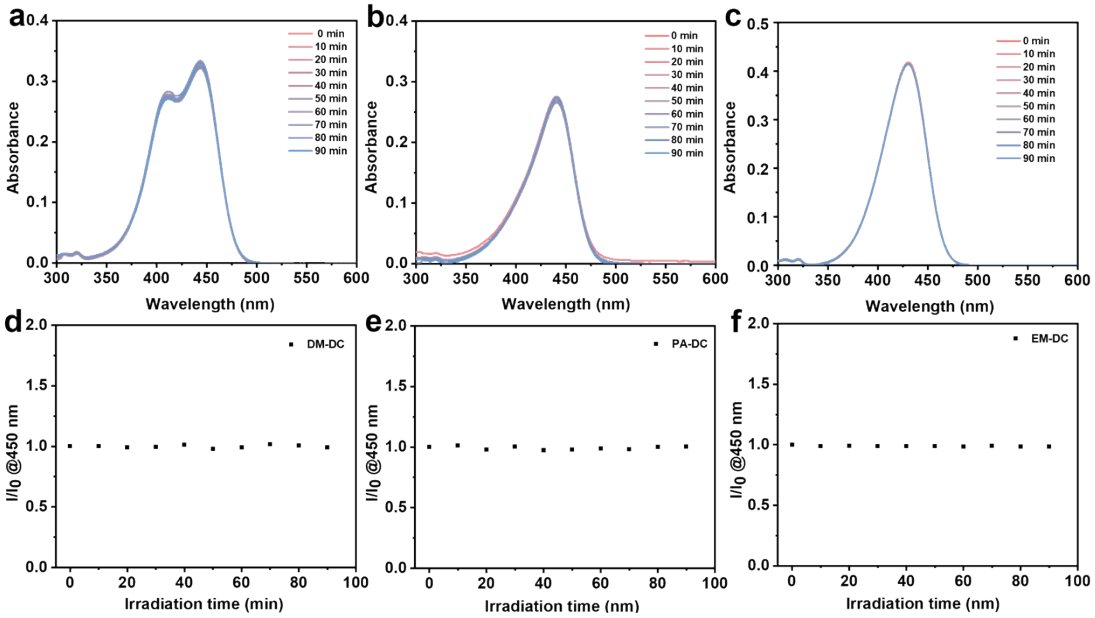


**Fig. S29** Absorption spectra of DM-DC (a), PA-DC (b), and EM-DC (c) in acetonitrile solution under white light (35 mW·cm$^{-2}$) irradiation for 90 min (DM-DC, PA-DC, or EM-DC: 25 μM). Absorbance decay of DM-DC (d), PA-DC (e), and EM-DC (f) in acetonitrile solution under white light (35 mW·cm$^{-2}$) irradiation for 90 min.

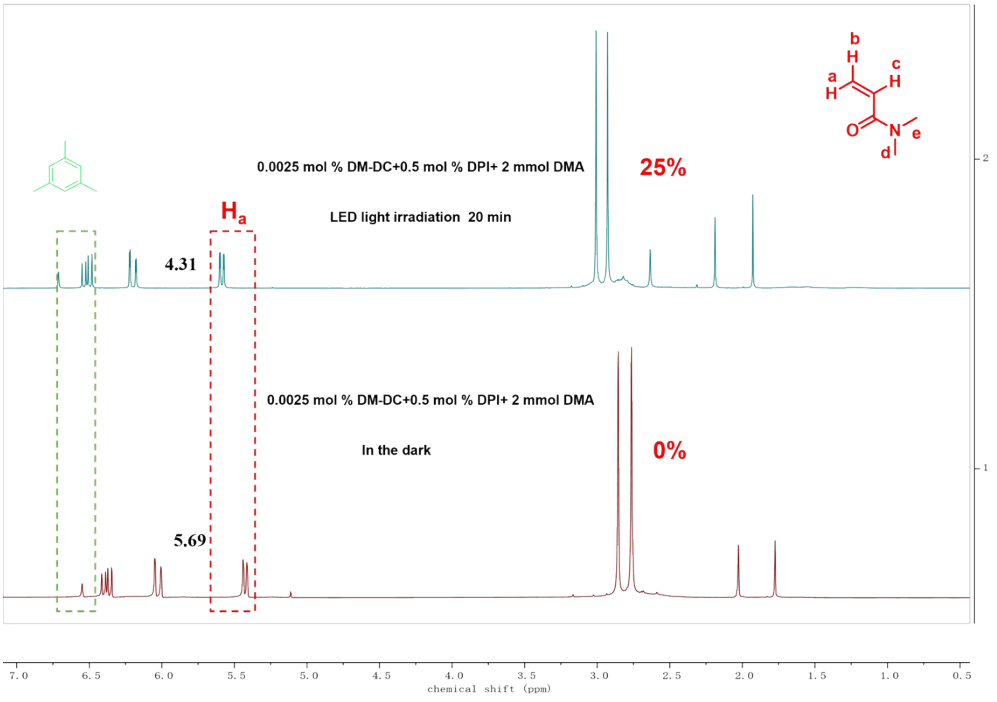


**Fig. S30** $^1$H NMR spectra of DMA in the presence of 0.0025 mol% DM-DC and DPI after 420-650 nm LED irradiation for 20 min and 0 min, in Ar, in $CDCl_3$.

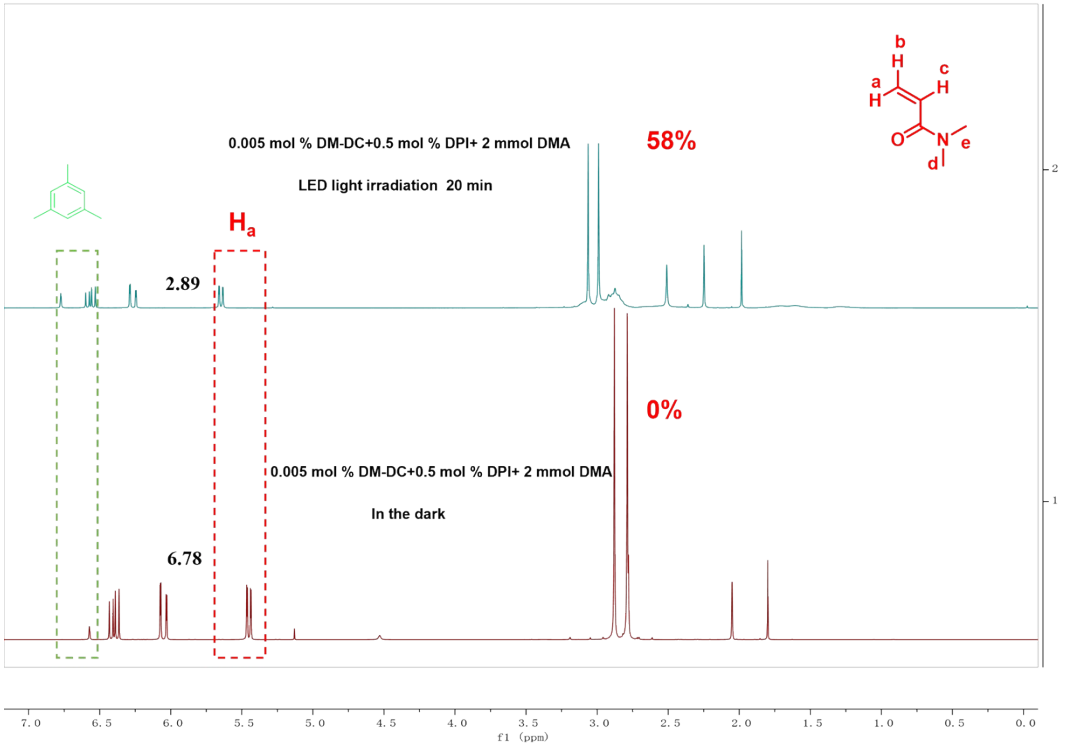


**Fig. S31** $^{1}$H NMR spectra of DMA in the presence of 0.005 mol% DM-DC and DPI after 420-650 nm LED irradiation for 20 min and 0 min, in Ar, in $CDCl_3$.

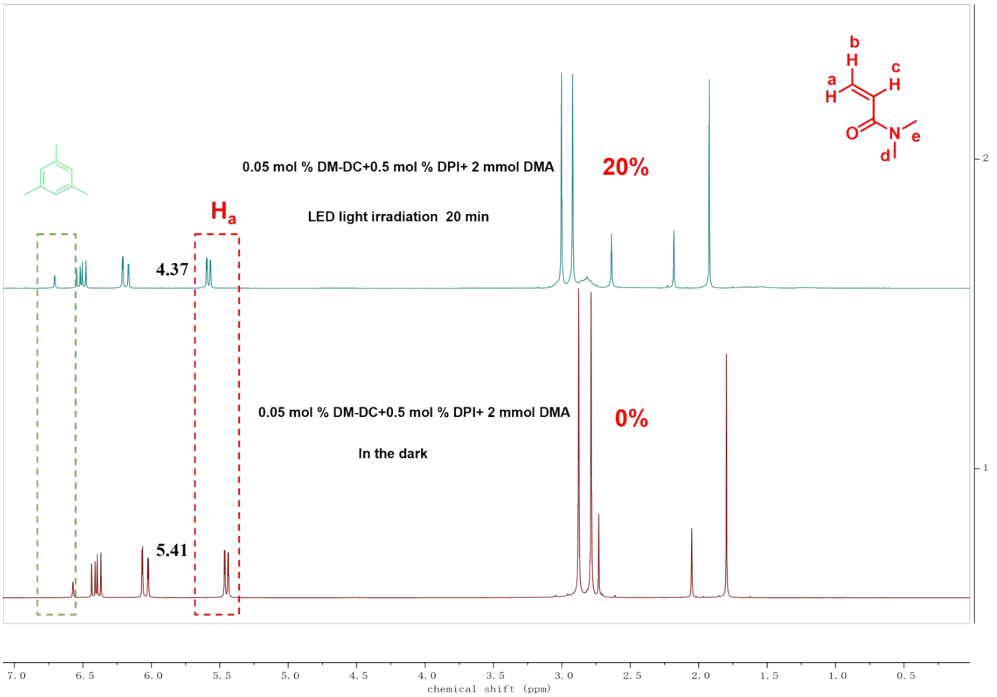


**Fig. S32** $^{1}$H NMR spectra of DMA in the presence of 0.05 mol% DM-DC and DPI after 420-650 nm LED irradiation for 20 min and 0 min, in Ar, in $CDCl_3$.

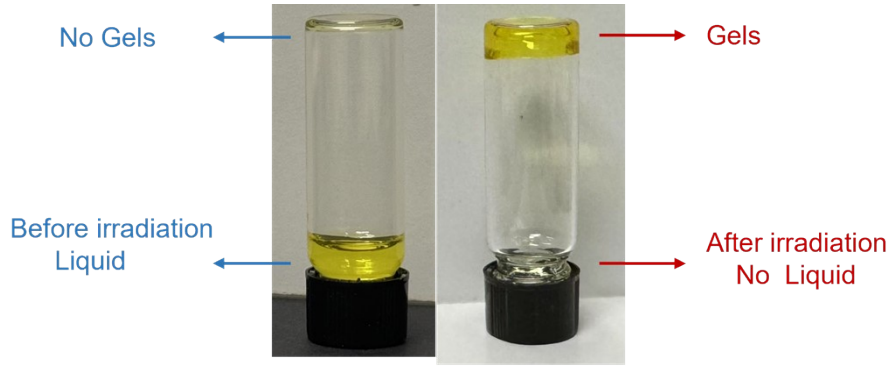


**0.01 mol % DM-DC+0.5 mol % DPI+ 2mmol DMA**

**Fig. S33** Photographs of the PDMA resin obtained by the photopolymerization method, showing the sample before and after light irradiation.

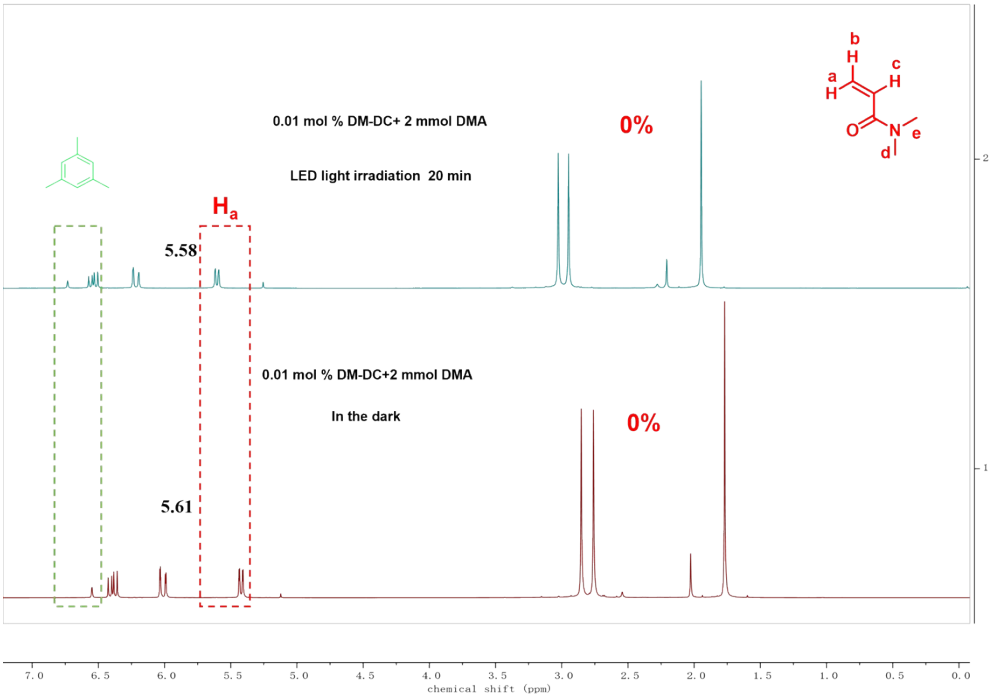


**Fig. S34** $^{1}H$ NMR spectra of DMA in the presence of 0.01 mol% DM-DC after 420-650 nm LED irradiation for 20 min and 0 min, in Ar, in $CDCl_3$.

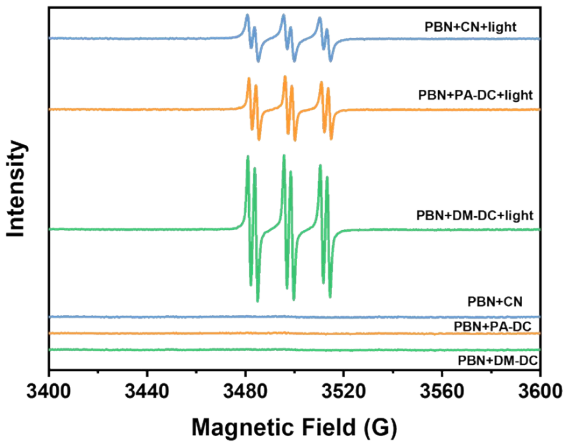


**Fig. S35** The EPR spectra of photocatalysts and photoinitiator by using PBN as radical scavenge.

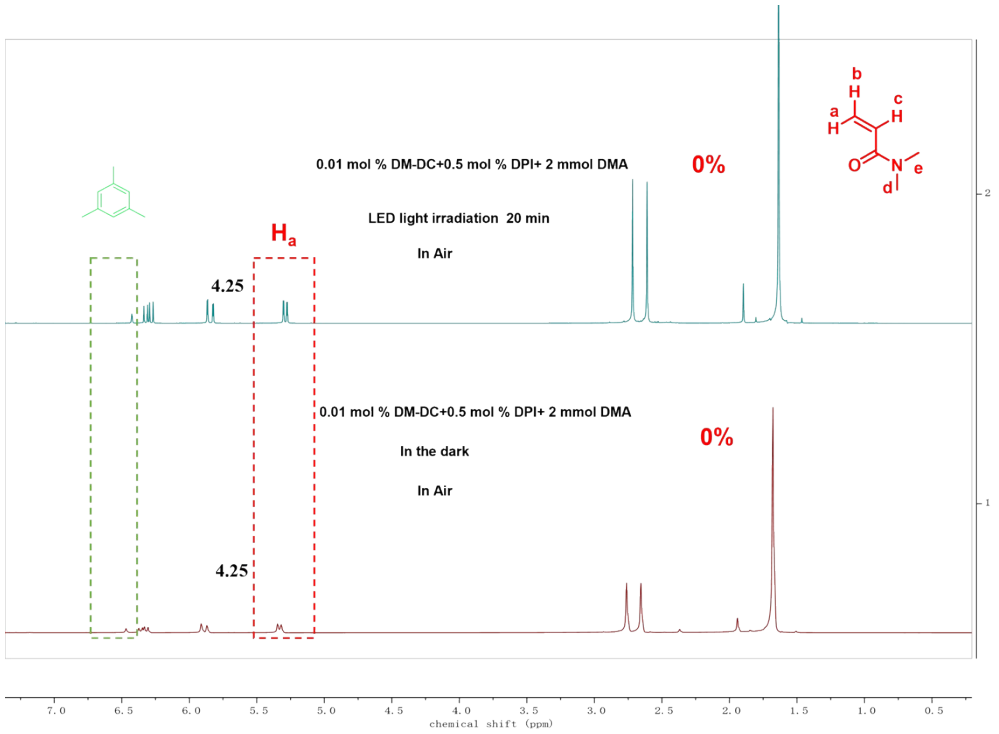


**Fig. S36** $^{1}H$ NMR spectra of DMA in the presence of 0.01 mol% DM-DC and DPI after 420-650 nm LED irradiation for 20 min and 0 min, in Air, in $CDCl_3$.

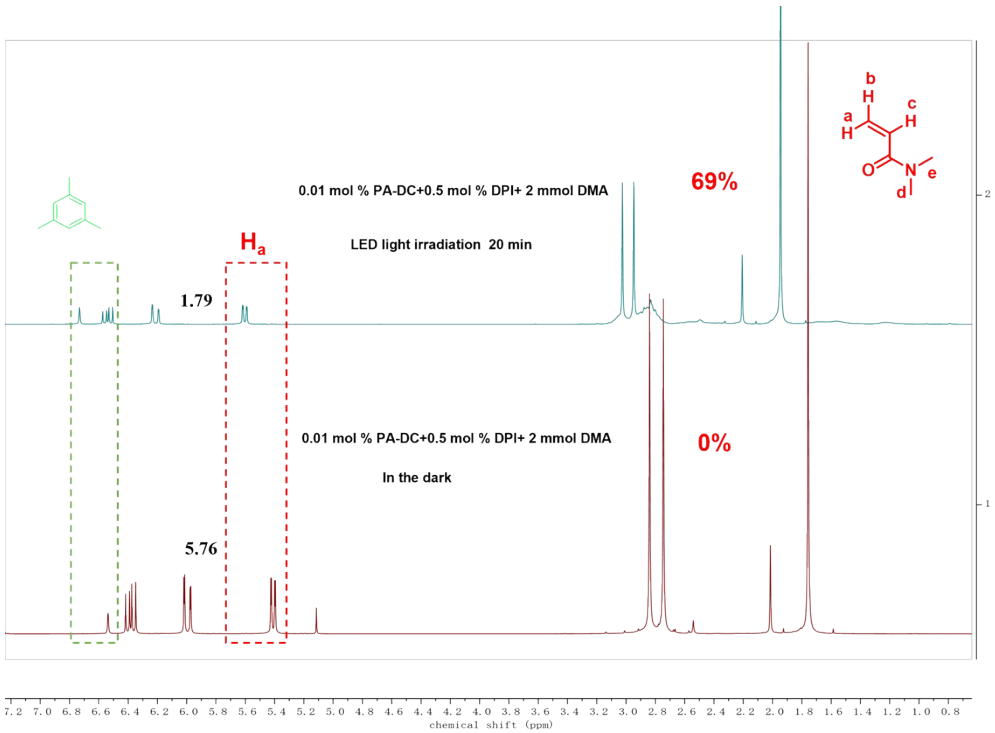


**Fig. S37** $^{1}$H NMR spectra of DMA in the presence of 0.01 mol% PA-DC and DPI after 420-650 nm LED irradiation for 20 min and 0 min, in Ar, in $CDCl_3$.

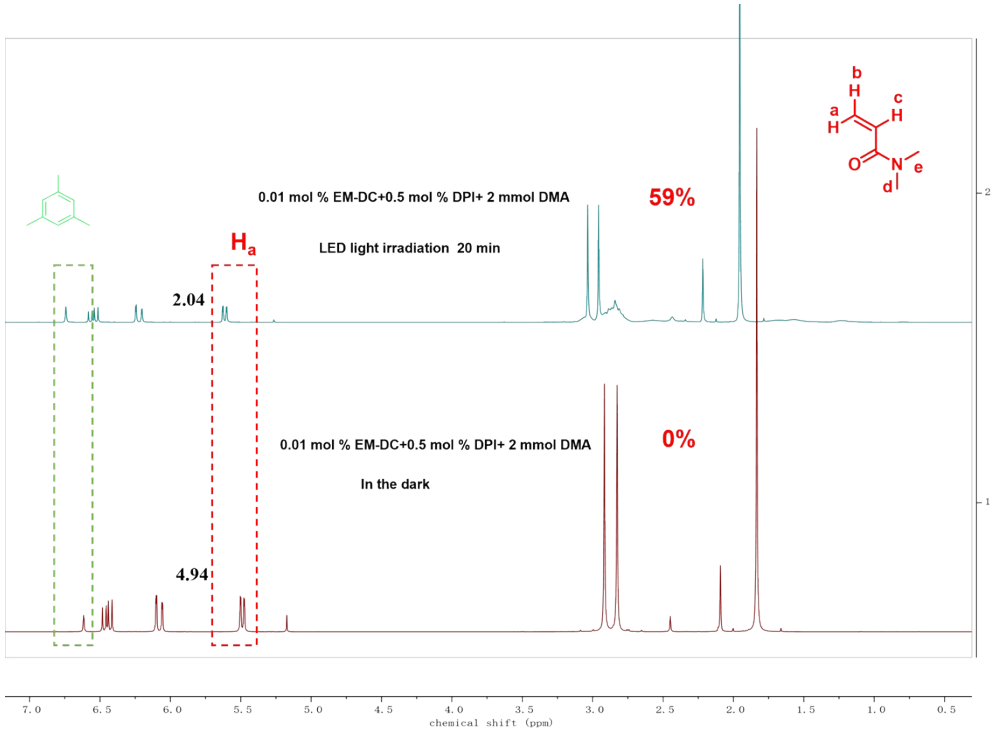


**Fig. S38** $^{1}$H NMR spectra of DMA in the presence of 0.01 mol% EM-DC and DPI after 420-650 nm LED irradiation for 20 min and 0 min, in Ar, in $CDCl_3$.

| Sample | $M_n$ (g $mol^{-1}$) | $M_w$ (g $mol^{-1}$) | $M_w/M_n$ |
|---|---|---|---|
| DM-DC | 39130 | 63090 | 1.612 |

**Table S2**. The molecular weight and dispersity values of the PDMA prepared by photopolymerization using DM-DC (0.01 mol %), DPI (0.5 mol %), and DMA (2 mM) after 420-650 nm (43 $mW \cdot cm^{-2}$) LED irradiation 20 min.

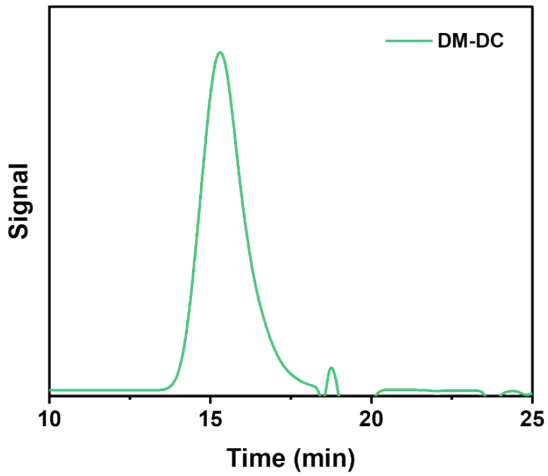


**Fig. S39** The GPC chromatograms of the PDMA prepared by photopolymerization using DM-DC (0.01 mol %), DPI (0.5 mol %), and DMA (2 mM) after 420-650 nm (43 mW·cm-2) LED irradiation 20 min.

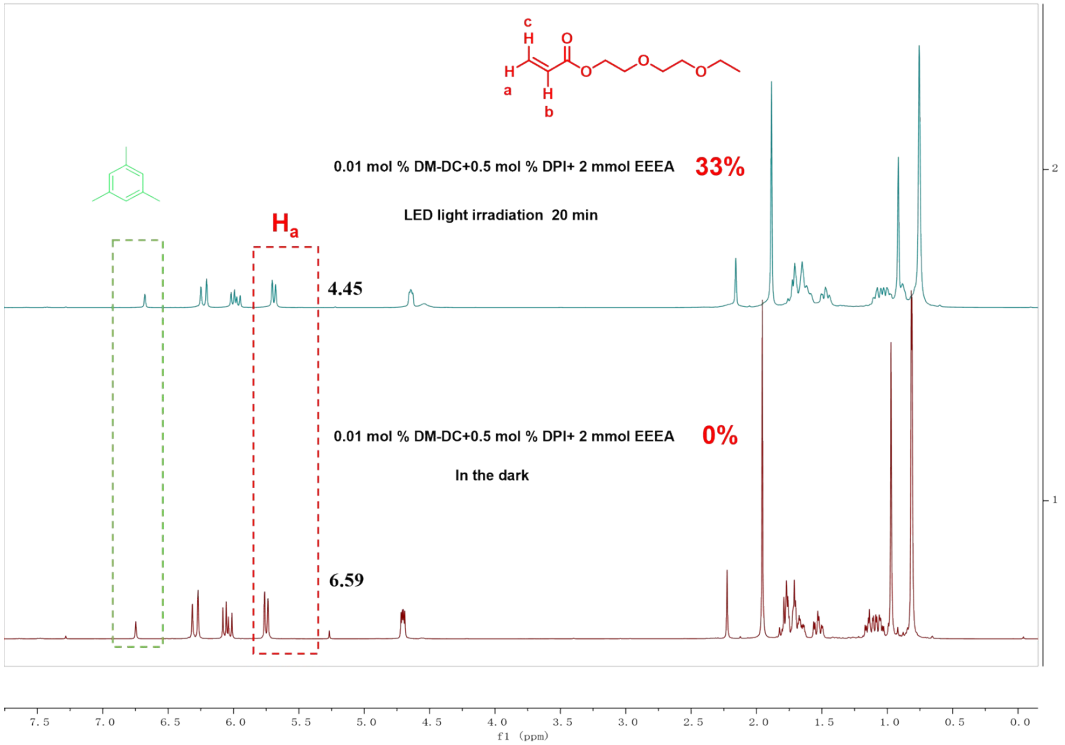


**Fig. S40** $^1H$ NMR spectra of EEEA in the presence of 0.01 mol% DM-DC and DPI

after 420-650 nm LED irradiation for 20 min and 0 min, in Ar, in $CDCl_3$.

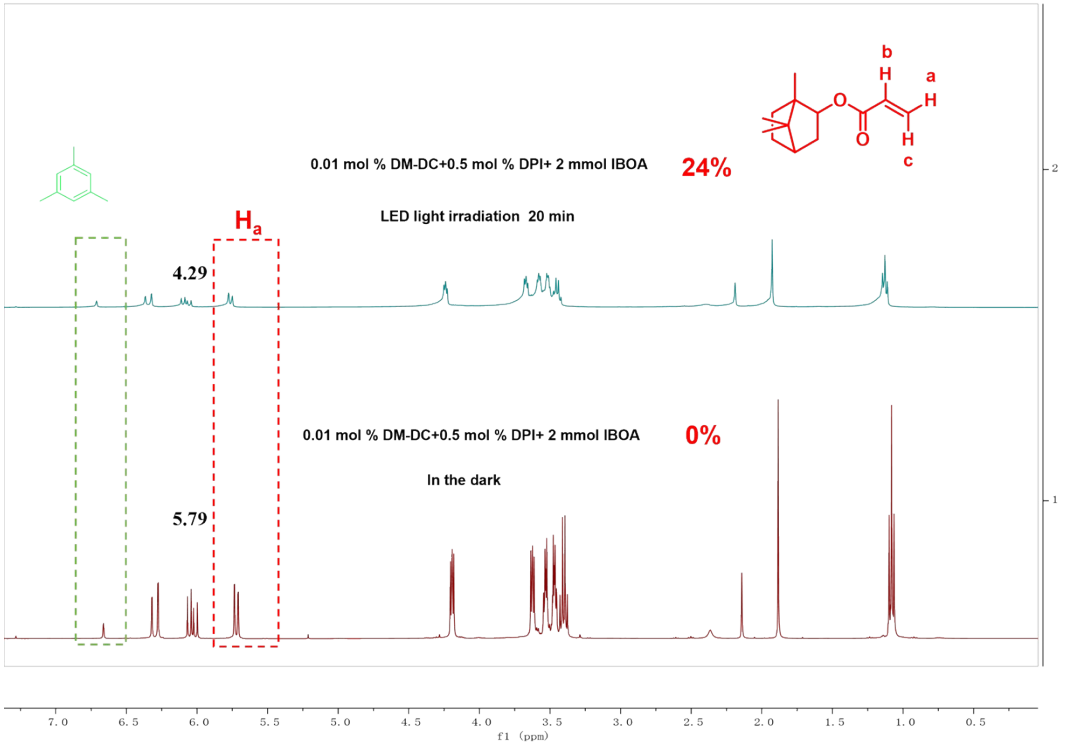


**Fig. S41** $^1H$ NMR spectra of IBOA in the presence of 0.01 mol% DM-DC and DPI after 420-650 nm LED irradiation for 20 min and 0 min, in Ar, in $CDCl_3$.

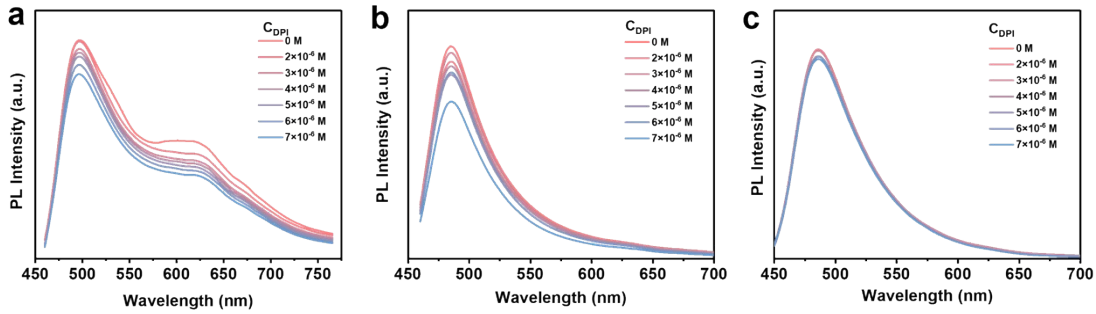


**Fig. S42** Fluorescence quenching curves of DM-DC (a), PA-DC (b), and EM-DC (c) ($c = 1\times10^{-5}$ M) by different concentration DPI. In acetonitrile.

[S1] Gaussian 09, Revision D.01, M. J. Frisch, G. W. Trucks, H. B. Schlegel, G. E. Scuseria, M. A. Robb, J. R. Cheeseman, G. Scalmani, V. Barone, B. Mennucci, G. A. Petersson, H. Nakatsuji, M. Caricato, X. Li, H. P. Hratchian, A. F. Izmaylov, J. Bloino, G. Zheng, J. L. Sonnenberg, M. Hada, M. Ehara, K. Toyota, R. Fukuda, J. Hasegawa, M. Ishida, T. Nakajima, Y. Honda, O. Kitao, H. Nakai, T. Vreven, J. A. Montgomery, Jr., J. E. Peralta, F. Ogliaro, M. Bearpark, J. J. Heyd, E. Brothers, K. N. Kudin, V. N. Staroverov, T. Keith, R. Kobayashi, J. Normand, K. Raghavachari, A. Rendell, J. C. Burant, S. S. Iyengar, J. Tomasi, M. Cossi, N. Rega, J. M. Millam, M. Klene, J. E. Knox, J. B. Cross, V. Bakken, C. Adamo, J. Jaramillo, R. Gomperts, R. E. Stratmann, O. Yazyev, A. J. Austin, R. Cammi, C. Pomelli, J. W. Ochterski, R. L. Martin, K. Morokuma, V. G. Zakrzewski, G. A. Voth, P. Salvador, J. J. Dannenberg, S. Dapprich, A. D. Daniels, O. Farkas, J. B. Foresman, J. V. Ortiz, J. Cioslowski, and D. J. Fox, Gaussian, Inc., Wallingford CT, **2013**.

[S2] S. Grimme, J. Antony, S. Ehrlich, H. Krieg, *J. Chem. Phys*. **2010**, *132*, 154104.

[S3] F. Weigend, R. Ahlrichs, Phys. *Chem. Chem. Phys*. **2005**, *7*, 3297.

[S4] S. Grimme, S. Ehrlich, L. Goerigk, *J. Comput. Chem*. **2011**, *32*, 1456-1465.

[S5] P. J. Stephens, F. J. Devlin, C. F. Chabalowski, M. J. Frisch, J. Phys. Chem. **1994**, *98*, 11623-11627.

[S6] B. Li, Z. Li, F. Guo, J. Song, X. Jiang, Y. Wang, S. Gao, J. Wang, X. Pang, L. Zhao, Y. Zhang, *ACS Appl. Mater. Interfaces.* **2020**, *12*, 14233-14243.

[S7] T. Lu and Q. Chen, *Chemistry–Methods*, **2021**, *1*, 231-239.

[S8] T. Lu, F. Chen, *J. Comput. Chem*. **2012**, *33,* 580-592.

[S9] T. Lu, *J. Chem. Phys.* **2024**, *161*, 082503.

[S10] W. Humphrey, A. Dalke,K. Schulten, *J. Mol. Graph.* **1996**, *14*, 33-38